Study of AC Interference Corrosion: Advanced Electrochemical Tests and Mitigation with Novel Simulations

F. BABAGHAYOU*, B. ZEGNINI and T. SEGHIER
A Laboratory for the Study and Development of Semiconductors and Dielectric Materials, Amar Telidji University Laghouat, Algeria
babag.fatiha@gmail.com

Abstract

The HV power lines sometimes share the same path with buried pipelines that are protected by an insulation coating and a cathodic protection (CP). However, neighbouring HV power lines induce an alternative current (AC) which causes corrosion damages on metallic structures known as the AC corrosion phenomena. In this study, we did an experimental investigation on a laboratory model, to realize electrochemical tests on a pipeline steel sample. Afterwards, we did a numerical simulation studies. Where, we studied the corrosion electrochemical reactions such as anodic process and cathodic process; i.e. the iron oxidation and the reduction of both the oxygen and the hydrogen. We have also simulated the CP, the AC corrosion and the deformation of the steel pipeline sample. At last, to remedy this problem, we developed a monitoring and correction program for optimizing the AC corrosion. The main novelty of our work resides in our experimental and numerical simulation results, which are in good agreement, and the development of a program for an automatic mitigation of AC Corrosion.

Keywords: AC interferences, AC corrosion, Cathodic protection, Electrochemical tests, Electrode, Electrolyte.

1. Introduction

The overhead high voltage power transmission lines influence buried pipelines by inducing AC, causing the perturbation of the cathodic protection (CP) [1], leading to severe corrosion damages.

The AC corrosion has become a problem only in the last thirty years, after the growth in the number of interference sources, such as the traction systems and AC-powered electrical transmission lines that share the same path with the buried pipelines for long distances, because of the space limitation imposed by private or governmental entities [2, 3].

1

In recent decades, the insulation capacity improvement of the cathodically protected pipe coatings has aggravated the AC corrosion problem: the passage to the usage of bitumen particularly polyethylene and polypropylene extruded, allowed the increase of the coating electrical resistivity and minimise the size and the defects occurrences. This was an advantage, because it reduced the delivered CP current, but caused high interfering AC densities at the defects area. Many authors considered this as one of the main reasons for the increase in the number of corrosion cases attributable to AC interference [2, 4], and many researchers have carried substantial studies in this field such as A. Brenna *et al.* [2, 5], G.C. Christoforidis *et al.* [4], E.S.M. Nicoletti [6, 7], K. Dae–Kyeong *et al.* [8], L. V. Nielsen *et al.* [9, 10], Y. Hosokawa [11], Q. Ding *et al.* [12], I. Ibrahim *et al.* [13] and International Institute Nace [14].

Gas and oil companies have confronted serious pipelines AC corrosion problems, even in a protection condition by both an insulation coating and a cathodic protection (CP). To remedy the problem, companies need to replace defective sections, which is very costly.

In this work, to solve this problem, we aim to simulate this phenomenon and conduct investigations. First, we carried out electrochemical tests on a laboratory model, by using a sample of the pipeline steel type API 5L X52, which is used in Algeria. We used an advanced electrochemical workstation potentiostat and galvanostat EC–LAB VSP300, it allowed us to simplify the studied phenomenon model, and it provided all our measurements. We used a test cell containing a pipeline's sample, and a solution to simulate soil. Firstly, we subjected the test cell to free potential measurements, which means without both the CP and the AC, and then we applied a DC as CP to the sample. The measurements of the potential E_{off}, instant–off potential is the polarised half–cell potential of an electrode taken immediately after stopping the CP current, which closely approximates the potential without IR drop (i.e. the polarized potential) when the current was on. It allowed us to select an appropriate CP; then we added an AC in order to simulate the induced current. We did a numerical simulation study to represent digitally the test cell, the CP phenomenon and the AC corrosion. Moreover, we suggest an efficient solution for minimising its impact on pipelines. For this numerical simulation, we used the COMSOL Multiphysics software [15, 16]. We introduced all parameters of both of the iron sample and simulating the soil solution. We measured the E_{off}, we selected the appropriate CP, which brings the immunity state, and then we added AC for simulating the induced current. Finally, we have set up an automatic mitigation of AC corrosion by a monitoring and correction program to bring the E_{off}, in the AC presence, to the corrosion immunity zone, according to standards.
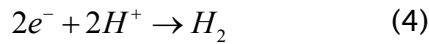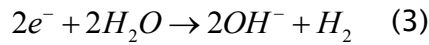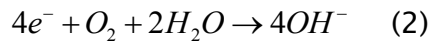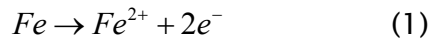
The optimization methods used in our work are the methods proposed by the COMSOL software for the Corrosion phenomenon and which are "Distribution of current in the cell", "Transport of diluted species" and "ODE / DAE" used for our program developed for the control and modification of CP.

2. Experimental Study

In order to do experimental investigation, we used an advanced electrochemical workstation potentiostat and galvanostat EC-LAB VSP300. It allowed us to simplify the studied phenomenon model, and it provided all of our measurements. We conducted the electrochemical tests on the laboratory model, we used a test cell containing an Iron sample of pipeline type API 5L X52, and a solution to simulate soil.

2.1. Electrochemical process

Below are the electrochemical process reactions [2, 8, 17]: Anodic Process (Eq. (1)) and Cathodic Process (Eq. (2), Eq. (3) and Eq. (4)):

$$Fe \rightarrow Fe^{2+} + 2e^- \qquad (1)$$

$$4e^- + O_2 + 2H_2O \rightarrow 4OH^- \quad (2)$$

$$2e^- + 2H_2O \rightarrow 2OH^- + H_2 \quad (3)$$

$$2e^- + 2H^+ \rightarrow H_2 \qquad (4)$$

2.2. Material and methods (electrode, electrolyte & measuring device)

The working electrode was API 5L X52 steel used in Algeria with the following chemical composition: 0.31% Manganese, 1.35% Carbon, 0.030% Sulphur and 0.030% Phosphor. (as shown in Fig. 1). The electrode is a metallic conductor, thus its potential relation [2, 18]:

$$\Phi_s = E_{CP} + E_{AC} = E_{CP} + A.\sin\left(2.\pi.f.t\right) \qquad (5)$$

where, E_{CP} is the applied potential of CP, E_{AC} is the AC potential, A is the amplitude of the AC potential and f is the frequency (50 Hz).

The electrolyte is composed by a soil-simulating solution [2, 4]: 200 mg/L chlorides (0.33 g/L of $NaCl$) and 500 mg/L sulphate ions (0.74 g/L of Na_2SO_4). It was prepared from distilled water and analytical grade reagent for the electrochemical tests.

The Measuring device is the potentiostat and galvanostat EC-LAB VSP300 for applying DC (CP) and AC simultaneously to the sample (Fig. 1). The EC-Lab VSP300 provides useful

techniques separated into two categories Electrochemical Techniques and Electrochemical Applications [18].

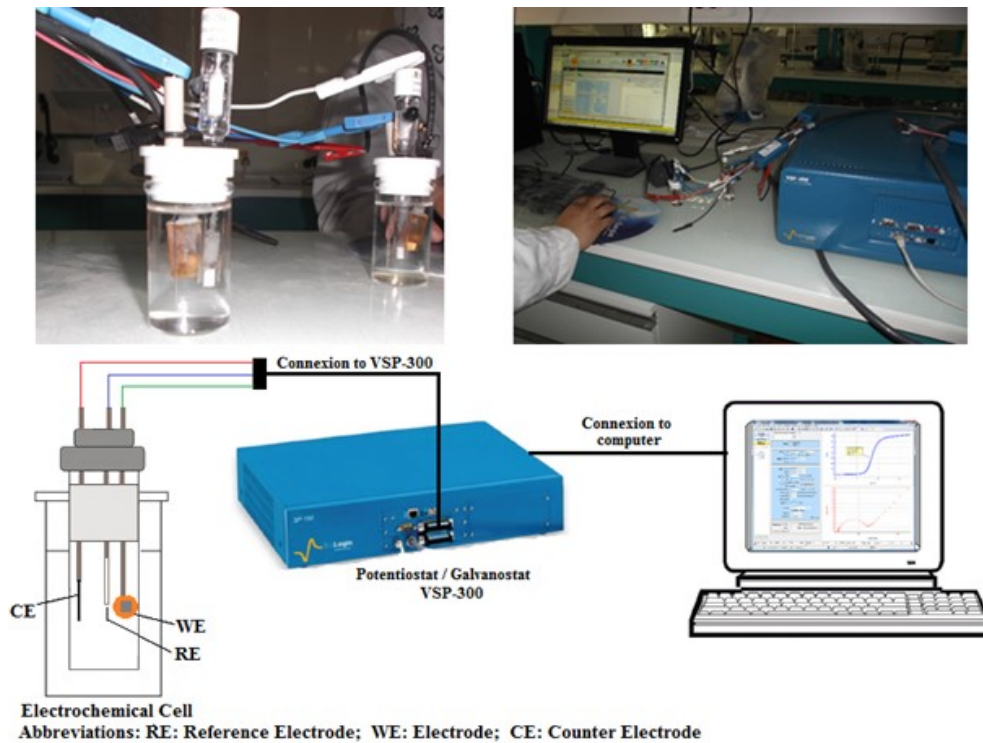Fig. 1 show a schematic experimental setup diagram of AC corrosion of pipeline steel.

Figure 1: Cell – Sample, Electrolyte ($NaCl$, Na_2SO_4), Reference electrode (Cu/CuSO$_4$) [8], Counter electrode.

2.3. Steps of the experimental tests

We followed the below steps for carrying out the experimental tests:

Step 1: We used the free-potential procedure, to highlight the corrosion process in the absence of PC and AC.

Step 2: We applied the linear polarization method, to find the area where the sample did not oxidize, which we called the immunity zone.

Step 3: We selected the appropriate CP, where the E_{off} was in the immunity zone, in the absence of AC.

Step 4: We applied a variable value of the induced current (AC) and we measured the E_{off}, to underscore the overshooting of the restriction zone.

2.4. Results and discussion of experimental study

2.4.1 Free potential in the absence of CP and AC

This test aims to verify that, in the absence of CP (Free potential analysis method of VSP300 [18]), the sample undergoes oxidation.

The EC-Lab analysis software shows that without the CP, The potential decreases and stabilizes at −540 mV, the device also gives us E_{corr} = −540 mV and oxidation of the sample took place. The sample is in oxidation state.

2.4.2 The good immunity area and the adequate CP

We applied the LP analysis method (Linear Polarization Log i (E_{off})) [8, 18] on two different samples as showed in Fig. 2.

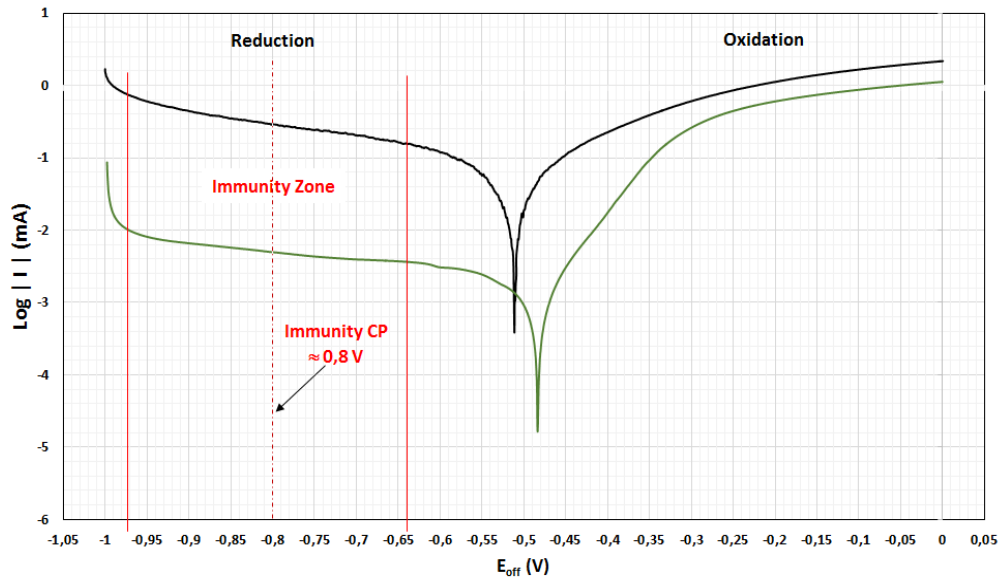This technique allows us to sweep in the same curve through both the reduction area and the oxidation zone.

Figure 2: Immunity zone and Adequate CP

In the reduction area, method illustrates the no-oxidation of iron samples part, i.e the reduction state. Then we can choose the immunity zone between −960 mV and −670 mV.

5

Regarding this results, we can also choose the adequate CP in the middle of the restraining zone, for our samples: CP ≈ −800 mV, which means for CP = −800 mV and −960 mV < E_{off} < −670 mV, the sample does not undergo any corrosion; it is in the immunity zone. Regarding tests results, they are consistent with the standards.

### 2.4.3 Application of an induced AC in the presence of CP

By applying the ACV technique (AC voltammetry VSP−300)18 and E_{off} potential monitoring, for several periods and different values of AC, we have the following results (showed in Fig. 3(a), Fig. 3(b) and Fig. 3(c)).

For CP = −800 mV and AC = 100 mV, the sample is in reduction state and E_{off} is in immunity area, it is illustrated by the green bar (the status green bar at the bottom left) as showed in Fig. 3(a).

For CP = −800 mV and AC = 200 mV or AC = 400 mV, the sample is in oxidation state and Eoff exceeded the immunity area, it is illustrated by the yellow bar (the status yellow bar at the bottom left) as showed in Fig. 3(b) and Fig. 3(c).

We can say that the use of the potentiostat and galvanostat EC−LAB VSP−300 gives the opportunity to facilitate the studies on AC corrosion by the application of the two currents DC and AC at the same time on the sample, and it allowed us to present many applications and analytical techniques. The VSP−300 replaces circuitry and electrical schemes from previous experiments, the experimental apparatus is appropriate for the study, especially given that the main focus of the paper is not to develop a new experimental set up and facilities technique, but to demonstrate his compatibility devices. Unfortunately, the only problem with this type of device is that it is not possible to correct automatically the CP in case of an Eoff exceeding the immunity zone.
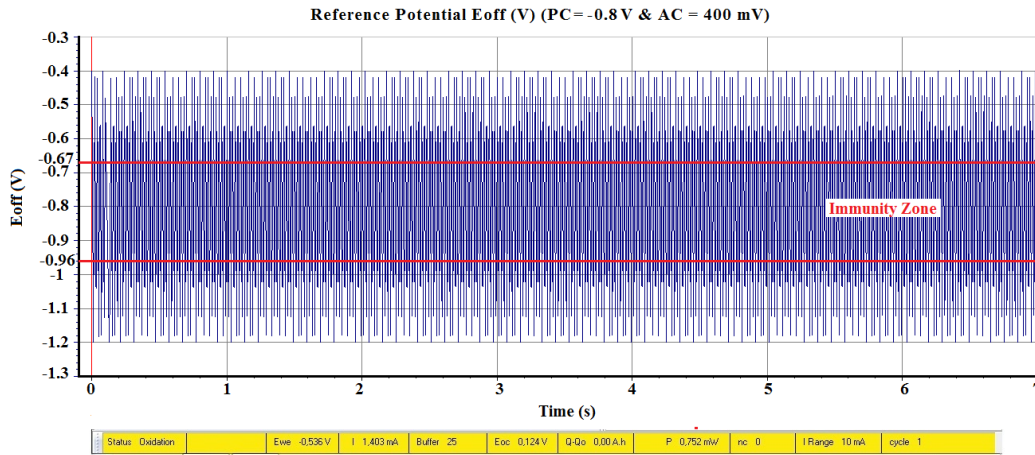
Therefore, we suggested a solution in the future perspective of this research.
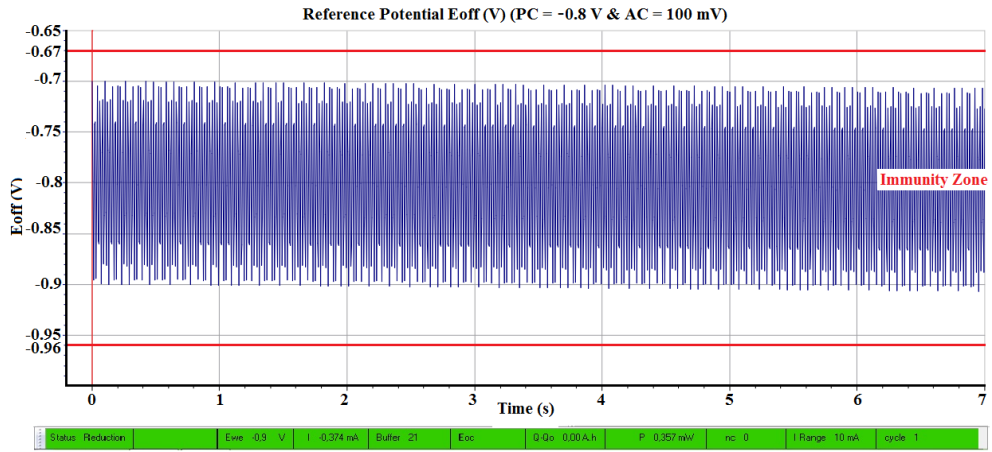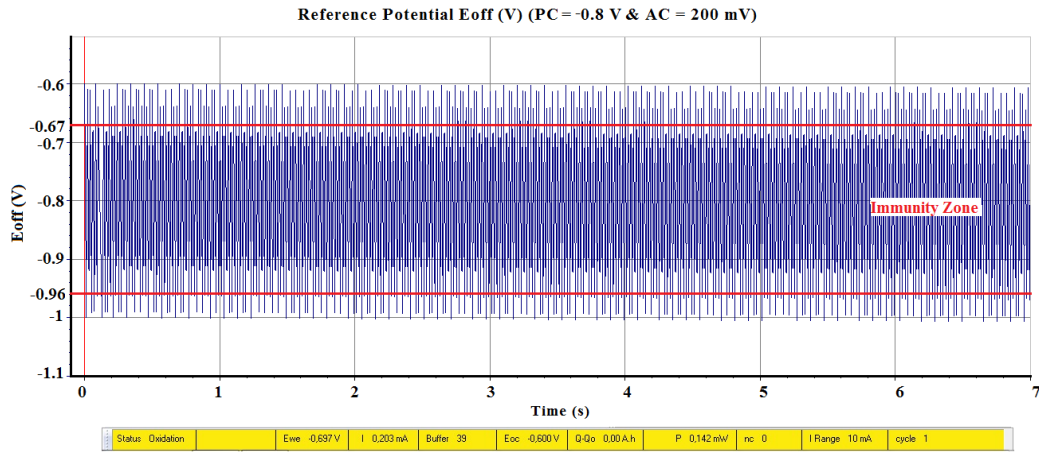
Figure 3: Potential E_{off} for CP=−800 mV (a) AC=100 mV, (b) AC=200 mV (c) AC=400 mV

7

3. Numerical Simulation

We ran a simulation study in order to digitally represent the CP phenomenon, AC corrosion and optimise AC corrosion behaviour, by changing the CP in the case of AC interferences. We developed a monitoring program that returns the process status to the immunity zone by referring to Pourbaix diagram and CP Hosokawa criteria [2, 11, 19].

The immunity zone is: -8.50 V $< E_{off} < -1.15$ V, where E_{off}, instant-off potential is the polarised half-cell potential of an electrode taken immediately after stopping the CP current, which closely approximates the potential without IR drop (i.e. the polarized potential) when the current was on.

Numerical simulations are based on:

3.1. The Model Geometry

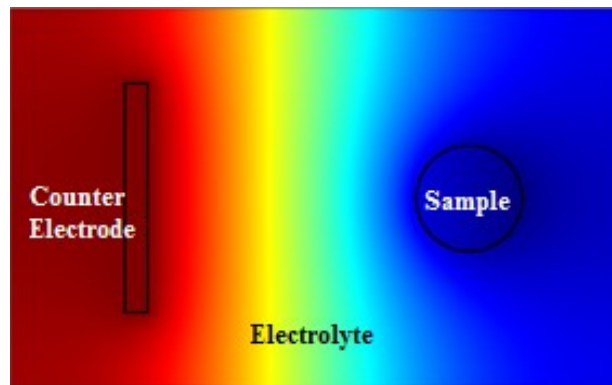Figure 4 shown the geometry model used.

Figure 4: The Model Geometry: Sample, Counter Electrode and Electrolyte

This simulation required [15, 16]:

The parameters initial value configuration of:

- The electrolyte conductivity, diffusion coefficient of Fe (Iron), O_2 (Oxygen) and H_2 (Hydrogen), Tafel slope iron oxidation, hydrogen evolution and oxygen reduction, reference concentration of Fe, O_2 and H_2, iron oxidation equilibrium potential, hydrogen evolution equilibrium potential, oxygen reduction equilibrium potential, iron oxidation exchange current density, hydrogen evolution current density, oxygen reduction exchange current density.

- The definition of the electrochemical composition of iron API 5L X52 pipeline used in Algeria (sample in Fig. 4) in the "Material Overview" Comsol section.

- The Definition of the reference electrode (measurement E_{off}) in the "Definitions-Domain Probe" Comsol section.

3.2. The parameterization of current distribution in the cell

The electrode is a metallic conductor; thus, its current-voltage relation obeyed to Ohm's law [20, 21]:

$$i_s = -\sigma_s \nabla \Phi_s \qquad \text{with} \qquad \nabla i_s = Q_s \qquad (6)$$

where is i_s the current density (A/m²) in the electrode, σ_s is the conductivity (S/m), Φ_s is the electric potential (V), and Q_s is the general current source term (A/m³).

The definition of the electric potential Φ_s is [2, 18]:

$$\Phi_s = E_{CP} + E_{AC} = E_{CP} + A.\sin(2.\pi.f.t) \qquad (7)$$

where E_{CP} is the applied potential of CP, E_{AC} is the induced AC potential, A is the amplitude of the induced AC potential and f is the frequency (50 Hz).

The electrolyte is an ionic conductor; thus, the net current density can be described using the sum of all ions fluxes:

$$i_l = F\sum_i z_i N_i \qquad (8)$$

where i_l is the current density (A/m²) in the electrolyte, F is Faraday constant (C/mol), and N_i is the flux of species i (mol.(m²/s)) with charge number z_i [19, 21].

The Nernst-Planck equation described the ion flux in an ideal electrolyte solution. This ion flux explains the flux of solute species by diffusion, migration and convection in the respective additive terms [19, 21]:

$$N_i = -D_i \nabla c_i - z_i u_{m,i} F c_i \nabla \Phi_l + c_i u \qquad (9)$$

where for the species i, c_i is the concentration (mol/m³), D_i is the diffusion coefficient (m²/s), $u_{m,i}$ is its mobility (s mol/kg), Φ_l is the electrolyte potential (V), and u is the velocity vector (m/s).

By substituting the Nernst-Planck equation into the expression for current density, we find [22]:

$$i_l = -F\left(\nabla \sum_i z_i D_i c_i\right) - F^2 \nabla \Phi_l \sum_i z_i^2 u_{m,i} c_i + uF \sum_i z_i c_i \qquad (10)$$

with current conservation: $\nabla i_l = Q_l$

This widespread treatment of electrochemical theory is generally too complicated to be practical. Supposing that one or more of the terms in Eq. (9) are weak, the equations can be simplified and linearized [19–21, 23, 24]:

$$i_l = -\sigma_l \nabla \Phi_l \quad \text{with} \quad \nabla i_l = Q_l \qquad (11)$$

The activation overpotential η (Electrode–Electrolyte–Interface) is the difference between the actual potential difference and the equilibrium potential difference [21–24]:

$$\eta = Q_s - Q_l - E_{eq} \qquad (12)$$

where E_{eq} is the equilibrium potential, and it is given by Nernst's equation[2]:

$$E_{eq} = E_0 + K \log\left(\frac{a_{M^{z+}}}{a_M}\right) \qquad (13)$$

where E_0 is the standard metal potential, K is a constant, a_{Mz+} is the metallic ions activity, a_M is the metal activity in the electrolyte.

3.3. The transport of chemical species

To configure the concentration and the chemical species movement (Fe, O_2, H_2), the driving forces for transport can be diffused by Fick´s law, convection when coupled to a flow field, and migration, when coupled to an electric field [21, 25].

$$(\sigma c_i / \sigma t) + \nabla\left(-D_i \nabla c_i\right) + u \nabla c_i = R_i \qquad (14)$$

where for the species i, c_i is the concentration (mol / m³), D_i is the diffusion coefficient (m²/s), u is the velocity vector (m/s), and R_i is the reaction rate expression (mol/(m³ s)).

The flux vector N (mol/(m² s)) is associated with the mass balance equation above and is used in boundary conditions and flux computations. For the case where the diffusion and convection are the only transport mechanisms, the flux vector is defined as [21]:

$$N_i = -D_i \nabla c_i + u c_i \qquad (15)$$

3.4. The math ODE and DAO Module

We used the module in COMSOL multi-physics to support the monitoring program to bring the situation to the immunity state, below the simplified algorithm used.

Beginning program

    read E_{eq}

    1: read E_{AC}, E_{CP}, E_{off}

    if ($E_{off} > -1.15$ V and $E_{off} < -0.85$ V) goto 1

      Calculate a new E_{CP} and other parameters

      Apply the new E_{CP} and the other parameters

    endif

    goto 1

end program

3.5. The sample deformation by corrosion

We applied on our model the Corrosion-Secondary a model wizard of Comsol [15, 16]. Which is a predefined multiphysics interface; it contains an interface for the electric current distribution and an interface for deformed geometry. The last handles the deformed geometry part of the problem.

For the counter electrode surface, which will not be deformed, we used an electrode surface node to model the reduction reaction. For the sample surface, we used an electrode surface node with an added dissolving-depositing species, which sets up both the deformation of the geometry and the steel electrode reactions.

We have also solved the model using a time-dependent study with automatic remeshing enabled [15, 16].

Afterwards, we described the reaction kinetics by the cathodic Tafel expression and the anodic electrode reaction current density by anodic Tafel expression [22, 26, 27]:

$$i_{cat} = -i_{0,cat} \times 10^{\frac{\eta}{A_{cat}}}, \qquad i_{tafel} = -i_{0,an} \times 10^{\frac{\eta}{A_{an}}} \qquad (16)$$

$$i_{an} = \frac{\left(i_{tafel} \times i_{\lim}\right)}{\left(i_{tafel} + i_{\lim}\right)} \qquad (17)$$

where i_0 is the exchange current density, η is the reaction overpotential, A_{an} and A_{cat} are the Tafel slope, and i_{lim} is the limiting current density.

The iron metal dissolution makes the electrode boundary moving, with a velocity in the normal direction, v (m/s), according to the formula:

$$v = \left(\frac{i_{an}}{2F}\right) \times \left(\frac{M}{\rho}\right) \qquad (18)$$

where M is the average molar mass, ρ is the iron density, F is the Faraday constant (C/mol).

3.6. The Boundary Condition

Our applied simulation obeyed to the boundary conditions below:

The boundary condition applied to the insulating surface is the potential gradient perpendicular to the surface and is equal to zero. The potential of the anode is fixed. The potential of the structure is assumed unknown and described on every point k by the equation:

$$U_k = V_k - E_{ok} - \eta_k\left(-\sigma\frac{\partial U_k}{\partial n}\right) \qquad (19)$$

where U_k is the potential in the soil adjacent to the point considered, V_k the potential of the metallic part of the structure, E_{ok} the Nernst potential of the metal–soil system, and $\eta_k\left(-\sigma\frac{\partial U_k}{\partial n}\right)$ the polarization voltage resulting from electrochemical reactions (mass and charge transport).

For coated structures, a linear voltage drop replaces the polarization across the coating resistance, featuring changing resistivity along the structures. When an AC voltage source is applied, it is necessary to implement the voltage as an explicit potential difference between two nodes lying on the surface of the protected structure and on the anode, respectively [15, 16].

3.7. Results and discussion of numerical modelling

3.7.1 The potential E_{off} in the presence of CP

Figures 5, 6(a) and 6(b) represent the E_{off} in the CP presence and for different values of an induced AC without and with the automatic mitigation of AC Corrosion by the immunity program respectively. This representation allowed us to discuss the curves of the sample corrosion based on the standards [2, 11, 19].

Figure 5(a) represents the measured E_{off} in the presence of a right CP without the presence of induced AC, we brought the E_{off} in the immunity area by choosing the adequate CP, regarding the standards [2, 11, 19].

Figure 5(b) shows that the potential E_{off} in the CP and AC presence (Amplitude $A = 100$ mV) did not exceed the immunity zone, in this case, we did not need to modify the CP.
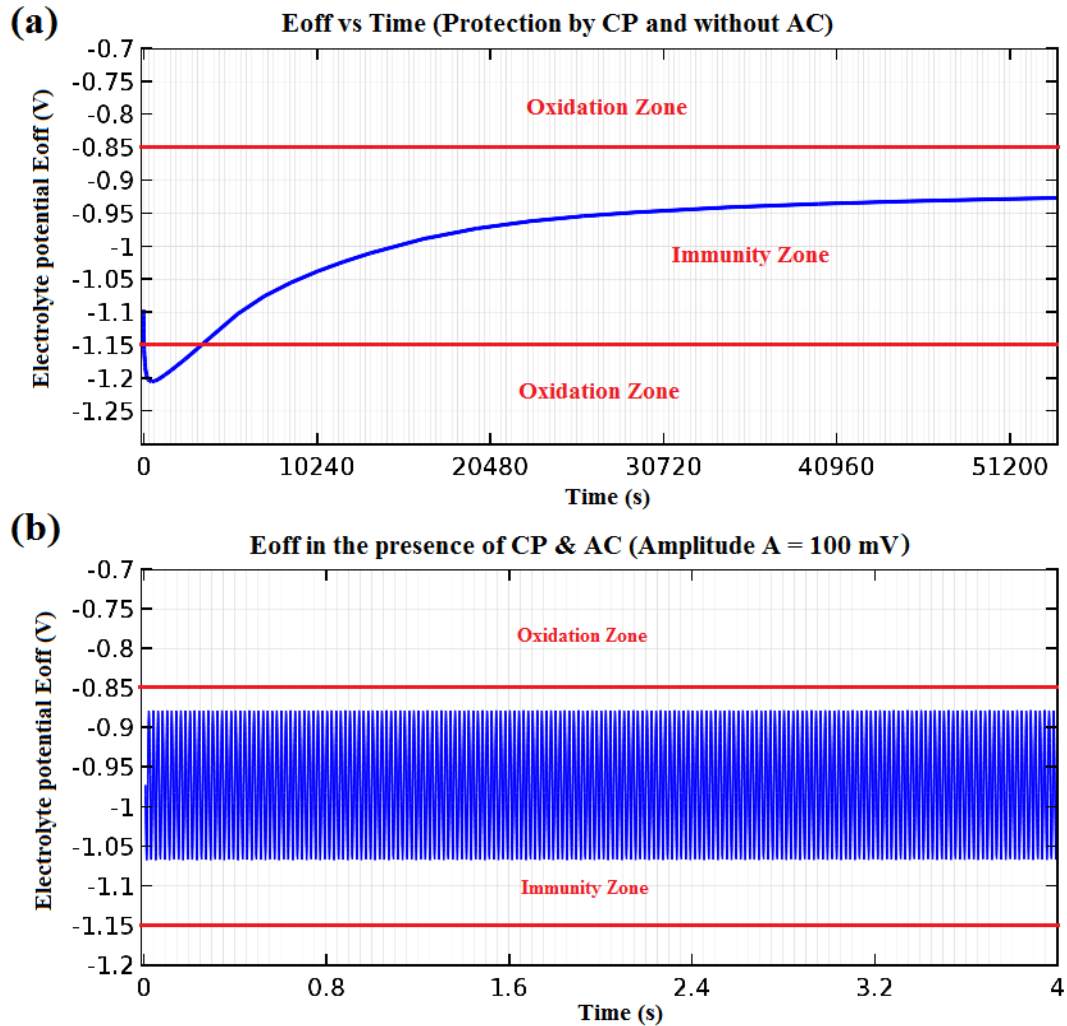

Figure 5: (a) E_{off} in the presence of CP (without AC), (b) E_{off} in the presence of CP & AC (Amplitude A=100 mV).

Figure 6 (Amplitude $A = 200$ mV) and Fig. 7 (Amplitude $A = 500$ mV) illustrate that E_{off} exceeded the immunity area; therefore, there is a significant corrosion risk. Then, for the same AC values and by introducing the automatic mitigation of AC Corrosion by the immunity program resolution (ODE / DAO), we were able to bring the E_{off} to the immunity

13

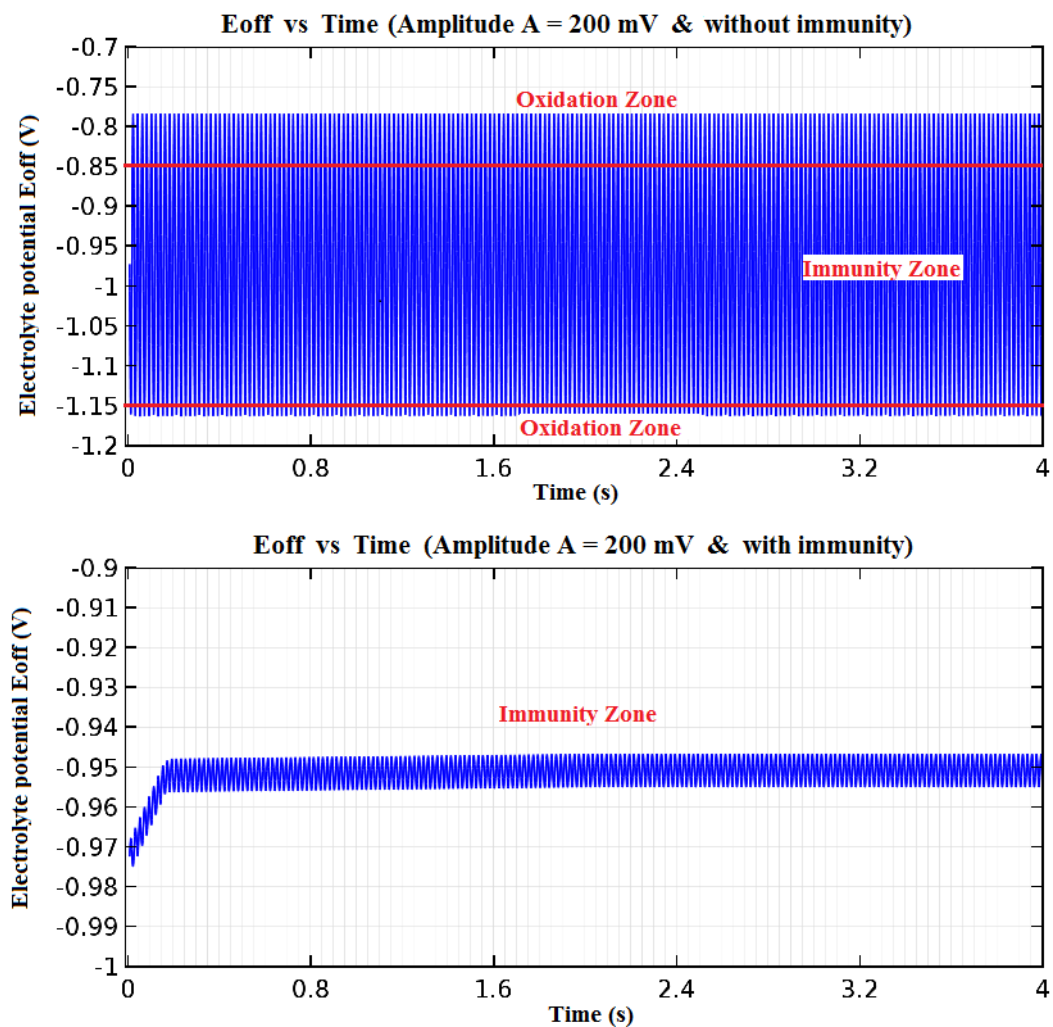zone. Secondly, we measured the different species concentration of the electrochemical process.

Figure 6: E_{off} in the presence of CP & AC (Amplitude A = 200 mV
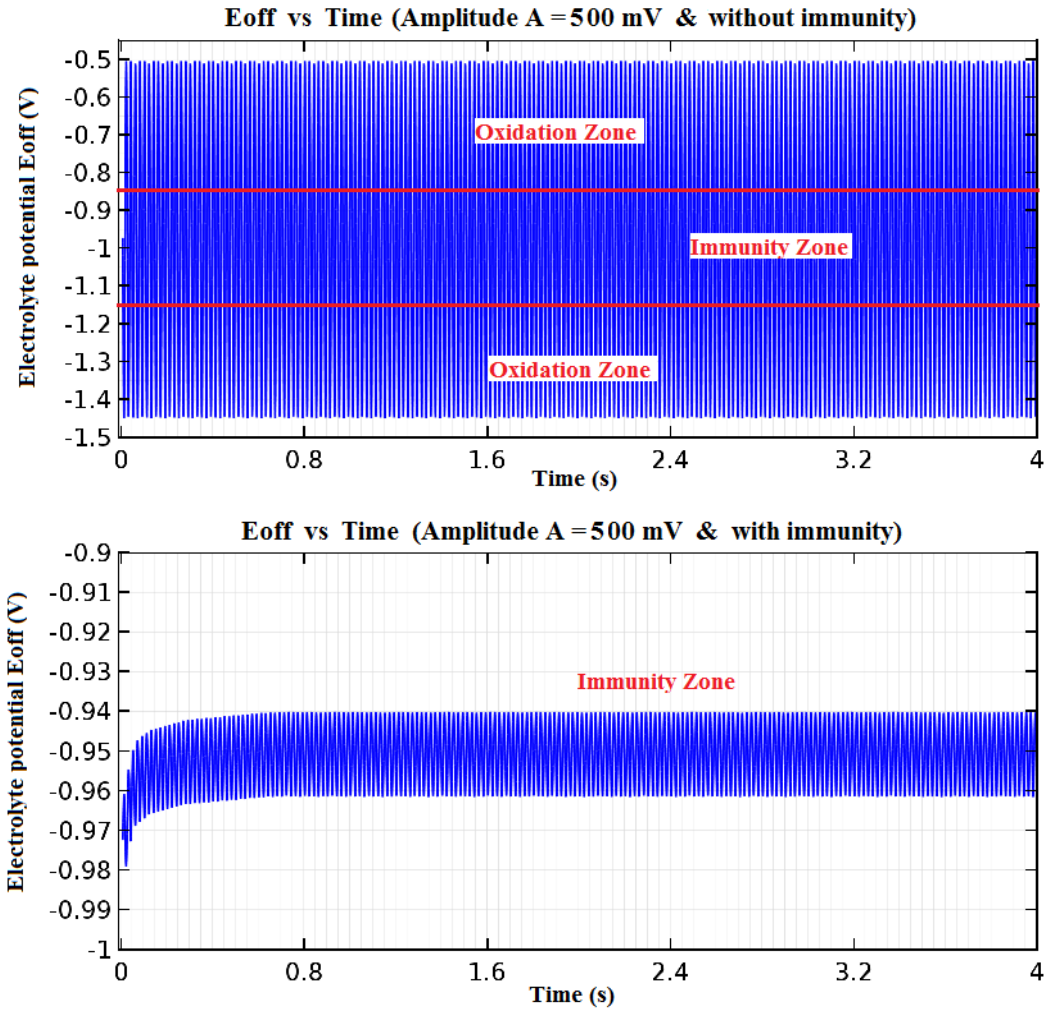
Figure 7: E_{off} in the presence of CP & AC (Amplitude A = 500 mV)

3.7.2 The Concentration of iron ions Fe^{2+}, Oxygen O_2 and Hydrogen H_2

Figure 8(a) shows the Iron ions Fe^{2+} concentration increase near the sample, thus, demonstrating that a reaction of iron oxidation (Eq. (1)) corrosion took place. After the implementation of the automatic mitigation of AC Corrosion by the immunity program, this concentration decreases.

Figure 8(b) illustrates the important Oxygen O_2 concentration decrease near the sample, thus, demonstrating a reaction of Oxygen reduction (Eq. (2)), implying that it is a case of a strong corrosion. After the implementation of the automatic mitigation of AC Corrosion by the immunity program, this concentration increases.

15

Figure 8(c) shows the Hydrogen H_2 concentration increase near the sample. It demonstrates that it is a reduction reaction of H_2O (Eq. (3)) or H^+ (Eq. (4)), indicating that a significant corrosion took place. After the automatic mitigation of AC Corrosion by the immunity program implementation, we notice a concentration decrease.
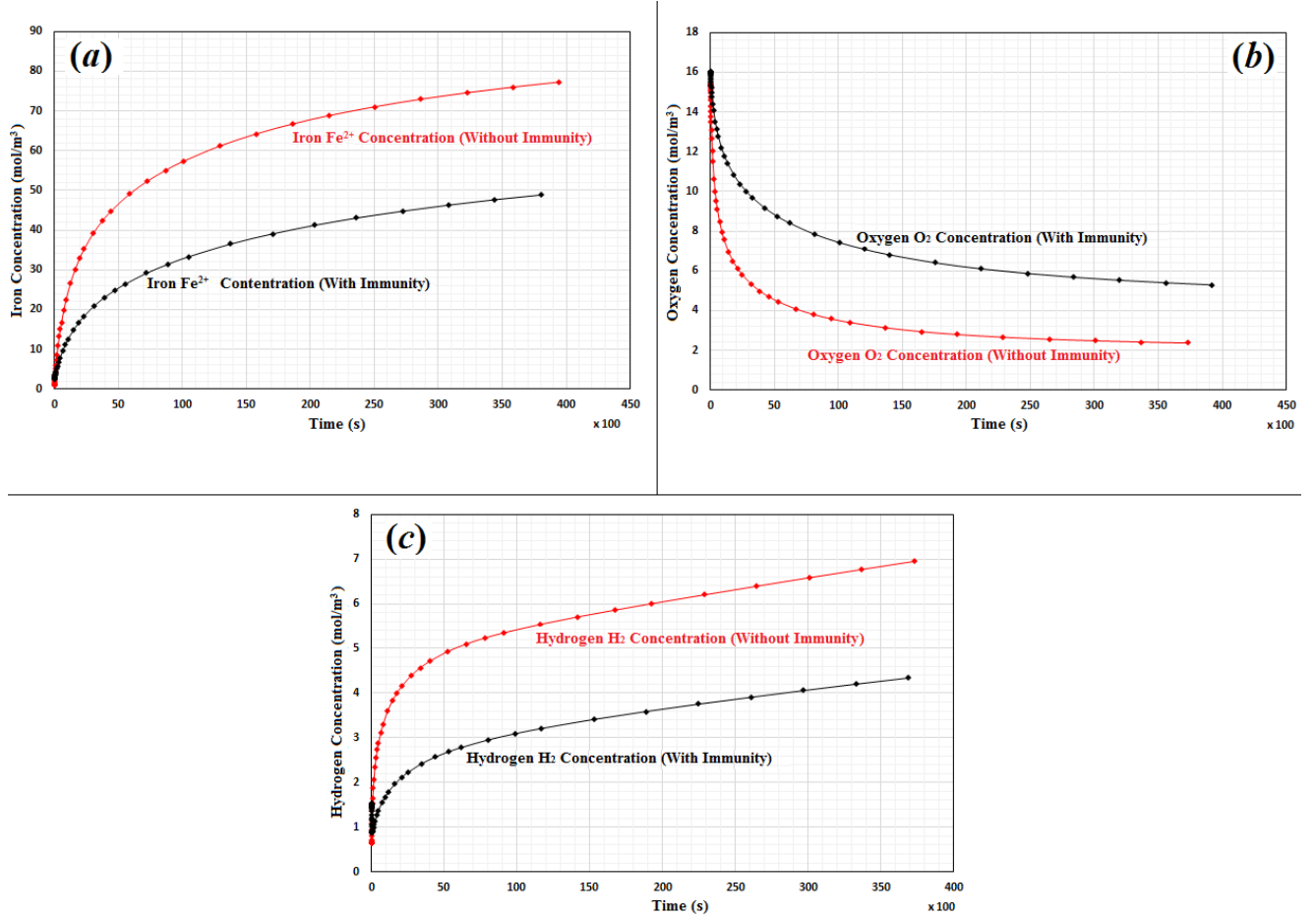
3.7.3 The Sample Deformation under CP and AC

Finally, we studied the sample deformation under both CP and AC.

Figure 8 illustrates the model geometry. We have presented a restriction of the electrolyte domain, to focus on the deformation area. The left part of the boundary is the surface of the counter electrode; the right part is the surface of the sample. On the right boundary a hole, of 0.1 mm deep, was created at the right of the geometry.
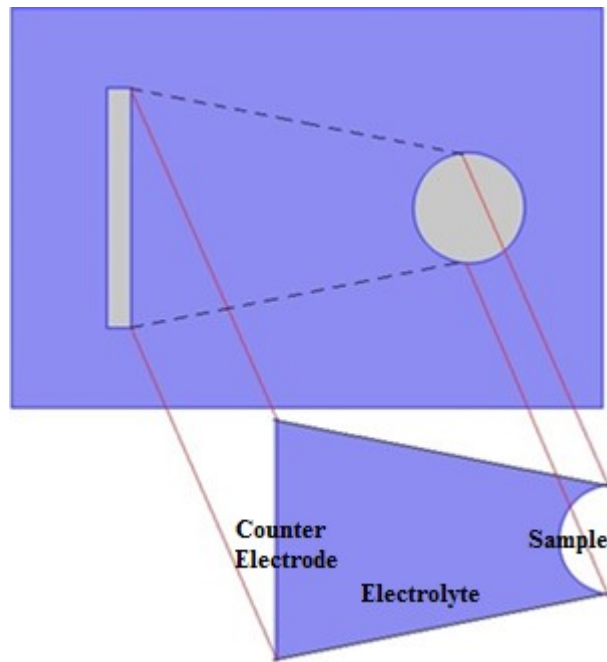
16

Figure 9: Model Restriction

Figure 9 illustrates the model restriction to show clearly the sample deformation.

Figure 10(a) shows, that when we introduce both CP and an induced AC during a period of 72 hours, corrosion makes a clear sample deformation, which has taken the shape of a hole, into the positive x direction of the geometry.

In Fig. 10(b), we executed the automatic mitigation of AC Corrosion by the rectification program during the same period (72 hours), and we did not observe any deformation.
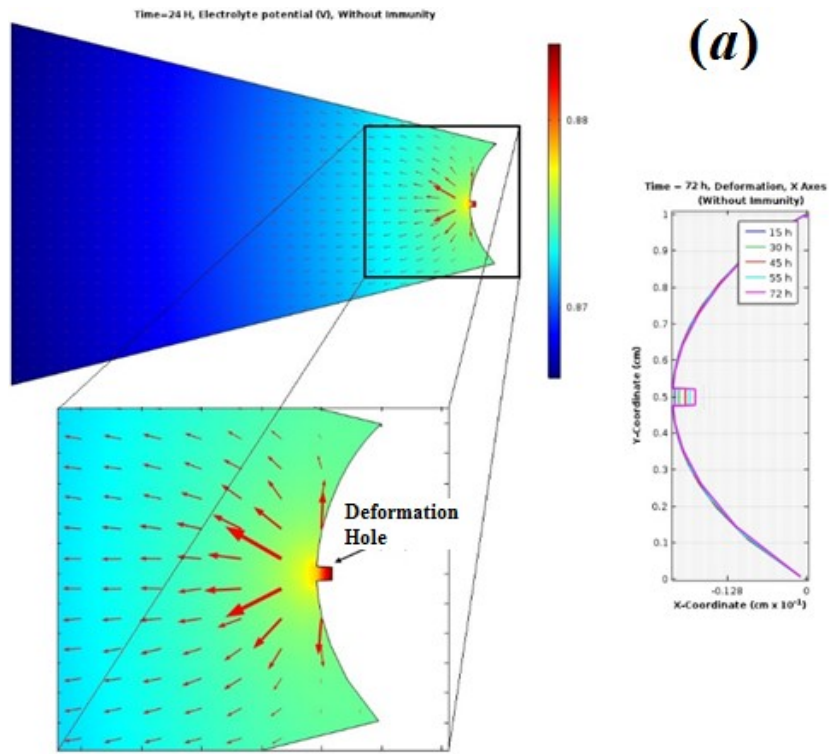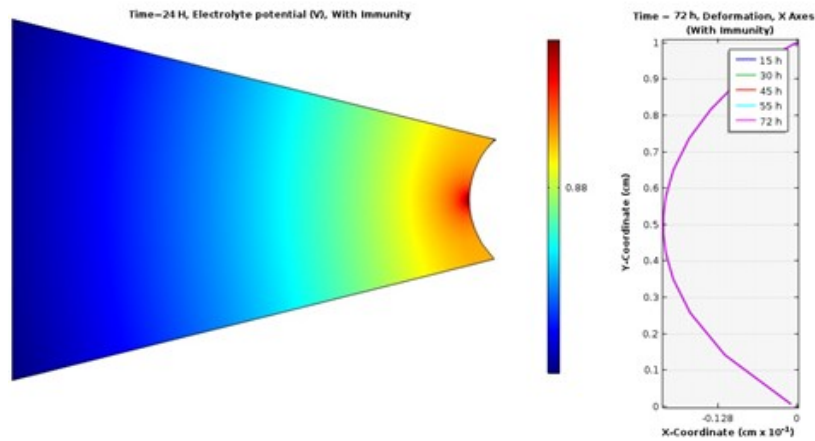
Figure 10: Sample Deformation by corrosion (under CP & AC) (a) Before implementation of the return program to the immunity zone (b) After implementation of the return program to the immunity zone.

4. The Comparison Between Experimental and Simulation Results

We would like to provide the direct links between the experimental and simulation study. We have used the same steel in the experiment and the one that was configured in the simulation (API 5L X52). The potential Φ_s applied to the studied sample in the experimental part obeyed to the formula Eq. (5), which is the same used in the numerical simulation Eq. (7). Fig. 3(a), Fig. 3(b) and Fig. 3(c) show that the experimental data are in good agreement with simulation results in Fig. 5(b), Fig. 6 and Fig. 7. The execution of the corrective program of CP in case of E_{off} exceeding the limits is possible in the simulation but experimentally it is not possible by the used device, the potentiostat and galvanostat.

5. Conclusions

In conclusion, in the practical study we modeled the AC corrosion phenomena. It allowed us; first, to record data such as the free potential, it showed that without the CP the sample was in oxidation state. Secondly, we have selected the proper CP in the absence of AC, by applying the LP analysis method (Linear Polarization: Log i (E_{off})) on two different samples, results have illustrated that for an adequate CP chosen in reduction area the sample does not undergo any corrosion, it was in the immunity zone, obtained tests results were consistent with the standards. Finally, the application of AC to the model protected by a CP, for low AC voltage, gave no oxidation because we did not exceed the immunity zone, and the sample was safe, but when AC increased, E_{off} exceeded the immunity area, and the oxidation took place. The numerical simulation's results indicated that the application of the induced AC causes sample corrosion, even under protection conditions. This was because we obtained an E_{off} exceeding the immunity zone combined with a heavy iron oxidation, a significant oxygen reduction, a high Hydrogen liberation and a clear sample deformation. Then by using our monitoring program, we were able to bring the E_{off} to the corrosion immunity zone according to standards when the AC was present. We were also able to decrease the electrochemical process reactions and equally to prevent the sample's corrosion. Because we had a clear deformation, in the form of a hole, of the sample by AC corrosion, then the use of the automatic mitigation by the rectification program during the same period 72 hours allowed us to avoid the deformation.

The direct links between the experimental and simulation study: we have used the same steel (API 5L X52). The potential applied to the studied sample obeys to the same formula; it was equal to the addition of a direct current as a CP and an alternating current as AC interference (Eq. (5) and Eq. (7)). The results have shown that the experimental data were

good agreement with the simulation ones. The monitoring and CP corrective program execution, when E_{off} exceeded the limits, was possible in the numerical simulation.

In our future perspective, our goal is to establish a microcontroller-based system to monitor the CP and to implement the immunity program along with the existing CP system in places where pipelines are near power lines and causing AC interferences.

Acknowledgments

References

[1] 'AC Corrosion on Cathodically Protected Pipelines: Guidelines for Risk Assessment and Mitigation Measures', L. D. Biase, CeoCor Committee edition, Luxembourg, 2001.

[2] 'Lightning Attachment Models and Maximum Shielding Failure Current of Overhead Transmission Lines: Implications in Insulation Coordination of Substations', A. Brenna, L. Lazzari, C. Castiglioni, Ph.D. Thesis, Politecnico, Milano Italy, 2012.

[3] 'New cathodic protection criteria based on direct and alternating current densities measured using coupons and their application to modern steel pipeline', Y. Hosokawa, F. Kajiyama, Y. J. Nakamura, in Proc. of Intern. NACE Corrosion Conf., 304-312, 2004.

[4] 'Inductive interference calculation on imperfect coated pipelines due to nearby faulted parallel transmission lines', G. C. Christoforidis, D. P. Labridis, *Electr. Pow. Syst. Res.* **66,** 2, pp139-148, 2003.

[5] 'Cathodic protection condition in the presence of AC interference', A. Brenna, L. Lazzari, M. Pedeferri, M. Ormellese, *La Metallurgia Italiana*, **6**, pp29-34, 2014.

[6] 'A pratical approach to pipeline corrosion modelling: part 1 – Long-term integrity forecasting', E. S. M. Nicoletti, R. D. Souza, S. C. Barros, *J. Pipeline Eng.* **8**, 1, pp19-28, 2009.

[7] 'A pratical approach to pipeline corrosion modelling: part 2 – Short-term integrity forecasting', E. S. M. Nicoletti, R. D. Souza, S. C. Barros, *J. Pipeline Eng.* **8**, 2, pp69-78, 2009.

[8] 'AC corrosion of mild steel in marine environments and the effects of cathodic protection', K. Dae-Kyeong, J.D. Scantlebury, S. Muralidharan, H. Tae-Hyun, B. Jeong-

Hyo, H. Yoon-Cheol, L. Hyun-Goo, J. of Corrosion Science and Engineering JCSE, Cathodic Protection, **9**, 12, University of Manchester in February 2006.

[9]   'AC induced corrosion in pipelines: detection, characterization and mitigation', L. V. Nielsen, K. V. Nielsen, B. Baumgarten, M. H. Breuning, P. Cohn, H. Rosenberg, in Proc. of International NACE Corrosion Conference, New Orleans, No. 04211, 2004.

[10] 'Role of alkalization in AC induced corrosion of pipelines and consequences hereof in relation to CP requirements', L.V. Nielsen, in Proc. of NACE Corrosion Conference, Houston, USA, no. 05788, 2005.

[11] 'Overcoming the new threat to pipeline integrity-AC corrosion assessment and its mitigation', Y. Hosokawa, F. Kajiyama, Y. Nakamura, in Proc. of International 23rd World Gas Conference, Amsterdam, Holland, No. 641, 2006.

[12] 'Experimental Study on the Influence of AC Stray Current on the Cathodic Protection of Buried Pipe', Q. Ding, Y. Fan, Int. J. Corr. **2016**, 561392, 2016.

[13] 'AC-Induced Corrosion of Underground Steel Pipelines Faradaic Rectification under Cathodic Protection: I. Theoretical Approach with Negligible Electrolyte Resistance', I. Ibrahim, T. Bernard, T. Hisasi, M. Michel, *J. Brazil. Chem. Soc.,* **26**, 1, pp196-208, 2015.

[14] SP0177, NS.: Standard Practice: Mitigation of Alternating Current and Lightning Effects on Metallic Structures Control System. NACE edition, Houston, 2007.

[15] Multiphysics C., Comsol Reference Guide, Comsol Multiph. Edition, 2012.

[16] 'Classical Models of the Interface between an Electrode and an Electrolyte', E. Gongadze, S. Petersen, U. Beck, U. Van-Rienen, in Proc. of International Comsol Conference, Milan, Italy, 14-16, 2009.

[17] 'AC corrosion - Case histories test procedures and mitigation', G. Wakelin, R. A. Gummow, S. M. Segall, in Proc. of International Conference NACE Corrosion. Houston, USA, no. 98565, 1998.

[18] BioLogic, EC-Lab., Software: Techniques and Applications. BioLogic Sience Instruments edition, 2011.

[19] 'CP3-Cathodic Protection', P. Nichols, B. Holtsbaum, D. Mayfield, S. Nelson, K. Parker, D. A. Schramm. NACE Tech. manual course, Houston, 2008.

[20] 'Apelian, Electric voltage predictions and correlation with density measurements in green-state powder metallurgy compacts', R. Ludwig, G. Leuenberger, S. Makarov, *J. nondestruct. Eval.* **21**, 1, pp1-8, 2002.

[21] 'Defects and Transport in crystalline solids', P. Kofstad, T. Norby, Compendium for the advanced level course, OSLO University, 2007.

[22] 'Effect of moisture on the spatial uniformity of cathodic protection of steel in reinforced concrete', E.B. Muehlenkamp, M.D. Koretsky, J.C. Westall, *Corrosion*, **61**, 6, pp519-533, 2012.

[23] 'Validated numerical modelling of galvanic corrosion for couples: Magnesium alloy (AE44)–mild steel and AE44–aluminium alloy (AA6063) in brine solution', K. B. Deshpande, *Corros. Sci.*, **52**, 10, pp3514–3522, 2010.

[24] 'Electrochemical Pickling of Steel for Industrial Applications: Modelling', M. Freda, A. Giannetti, L. Lattanzi, S. Luperi, in Proc. of International Excerpt from Comsol Conference, Rotterdam, Netherlands, 2013.

[25] 'Electrochemical Modelling of Cathodic Protection Systems Applied to Reinforced Concrete Structures'*,* E. B. Muehlenkamp, Thesis Oregon St. University USA, 2005.

[26] 'The Effect of Crevice-Opening Dimension on the Stability of Crevice Corrosion for Nickel in Sulfuric Acid', M. I. Abdulsalam, H. W. Pickering, *J. Electrochem. Soc.*, **145**, 7, 2276.18, 1998.

[27] 'Effect of aluminium spacer on galvanic corrosion between magnesium and mild steel using numerical model and SVET experiments', K. B. Deshpande, *Corros. Sci.*, **62,** pp184–191, 2012.